Supplementary Material

Table S1. Optical images acquired by the PlanetScope satellite for this study

Stage	Imaging Date (yyyy/mm/dd)	Instrument	Sun Elevation Angles (degree)	Sun Azimuth Angle (degree)
Pre-failure	2020/01/03	PS2	30.6	152.0
	2020/01/17	PS2	32.2	150.1
	2020/01/29	PS2	34.3	147.8
	2020/02/01	PS2	35.3	148.0
	2020/02/08	PS2	36.4	145.3
	2020/02/12	PS2	38.2	145.8
	2020/02/13	PS2	37.9	144.4
	2020/02/22	PS2	39.2	139.4
	2020/02/25	PS2	41.6	141.7
	2020/03/08	PS2	45.8	138.9
	2020/03/11	PS2	46.8	138.1
	2020/03/23	PS2	51.1	134.8
	2020/03/31	PS2	54.1	132.6
	2020/04/15	PS2	58.9	127.2
	2020/04/18	PS2	59.8	126.1
	2020/04/21	PS2	40.1	100.8
	2020/05/03	PS2	63.5	119.6
	2020/05/10	PS2	64.7	115.9
	2020/05/18	PS2	63.1	108.3
	2020/06/15	PS2	66.8	103.1
	2020/06/16	PS2	66.8	103.1
Post-failure	2020/06/24	PS2	69.0	105.5
	2020/07/26	PS2	64.0	110.3
	2020/07/27	PS2	38.3	89.2
	2020/08/19	PS2	60.2	122.2
	2020/08/25	PS2	59.2	125.5
	2020/08/27	PS2	58.7	126.7
	2020/08/28	PS2	58.3	127.0
	2020/09/04	PS2	57.0	131.6
	2020/09/21	PS2	52.7	140.2
	2020/10/15	PS2	45.5°	149.6
	2020/10/30	PS2	39.3	148.3
	2020/11/04	PS2	39.6	154.1
	2020/11/10	PS2	37.9	154.8
	2020/11/15	PS2	36.5	154.8
	2020/11/16	PS2	36.4	155.3
	2020/11/17	PS2	36.1	155.2
	2020/11/29	PS2	33.5	155.4
	2020/12/06	PS2	32.4	155.2
	2020/12/16	PS2	31.1	154.2
	2020/12/19	PS2	31.0	154.2
	2020/12/20	PS2	31.1	154.5
	2020/12/24	PS2	30.8	153.5

2020/12/27	PS2	30.7	153.2
2021/01/03	PS2	30.9	152.1
2021/01/04	PS2	30.9	152.0
2021/01/09	PS2	31.3	151.1
2021/01/10	PS2	29.5	146.8
2021/01/11	PS2	31.4	150.6
2021/01/29	PS2	34.5	147.7
2021/02/03	PS2	35.4	146.1
2021/02/06	PS2	37.2	147.8
2021/02/14	PS2	38.3	143.6
2021/02/22	PS2	40.7	142.0
2021/03/08	PS2	45.6	138.6
2021/03/09	PS2	45.9	138.1
2021/03/10	PS2	47.6	141.0
2021/03/24	PS2	51.4	134.4
2021/03/26	PS2	49.0	128.3
2021/04/09	PS2	56.9	129.5
2021/04/10	PS2	53.8	123.0
2021/04/20	PS2	56.3	118.5
2021/05/09	PS2	64.4	116.4
2021/06/02	PS2	66.9	106.3
2021/06/11	PS2	66.8	104.0

The initial and final window sizes test

The previous studies demonstrated that different combintations of the initial and final window sizes in the COSI-Corr method could lead to various displacement results [50]. In this work, different combinations of the initial and final window sizes were tested with the PlanetScope images for investigating the influence of window sizes of pixel offset tracking (POT) on the generated horizontal displacements. The correlated pair between 16 June 2020 and 24 June 2020 was selected for this test as these two images have similar sun illumination condition and construct relatively shorter temporal baseline, which could minimize the effect of shadows and temporal decorrelation. We used the red band for image correlation, and the step size is fixed to 2. Figure S1 shows the mean east-west and north-south displacements and the corresponding standard deviations (uncertainties) in the stable area of the generated POT result for different combinations of initial and final window sizes, as well as the measurement quality (SNR). The stable area is depicted as the orange rectangle in Figure S2.

These detected mean east-west and north-south displacements in the stable area are ranging between -0.2 and 0.2 m, which indicated these two PlanetScope images were well registered with each other. Obviously, the uncertainties for the larger final window sizes (64, 128, and 256) are much lower than thoes for smaller final window size (8, 16 and 32). Although the mean SNR (meaurement quality) over the stable area for all combintations are similar, the uncertainities for thoes with larger window sizes (both ≥ 64) are relatively smaller.

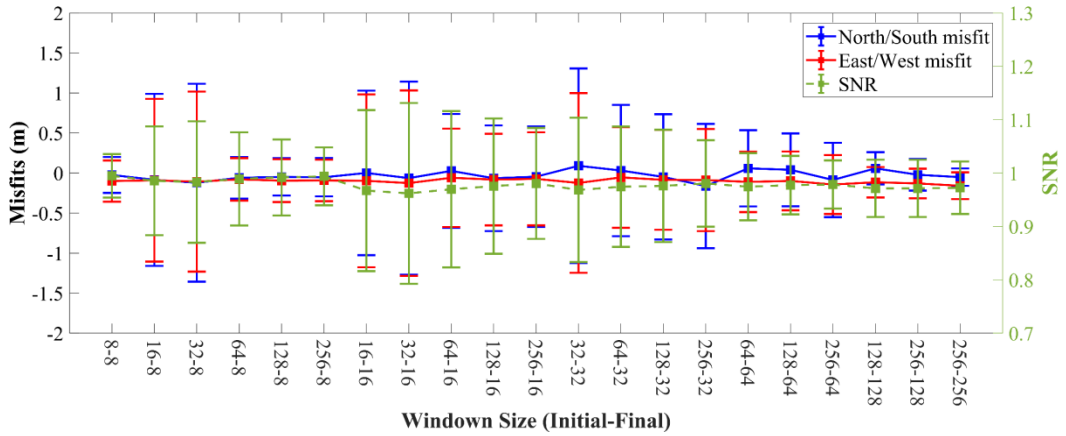


Figure S1. Means, standard deviations, and SNR (measurement quality) in the stable area of POT results derived from the PlanetScope image pair between 16 June 2020 and 24 June 2020 with different combinations of initial and final window sizes after filtering process. Note that fixed step size is 2 and the red band is used.

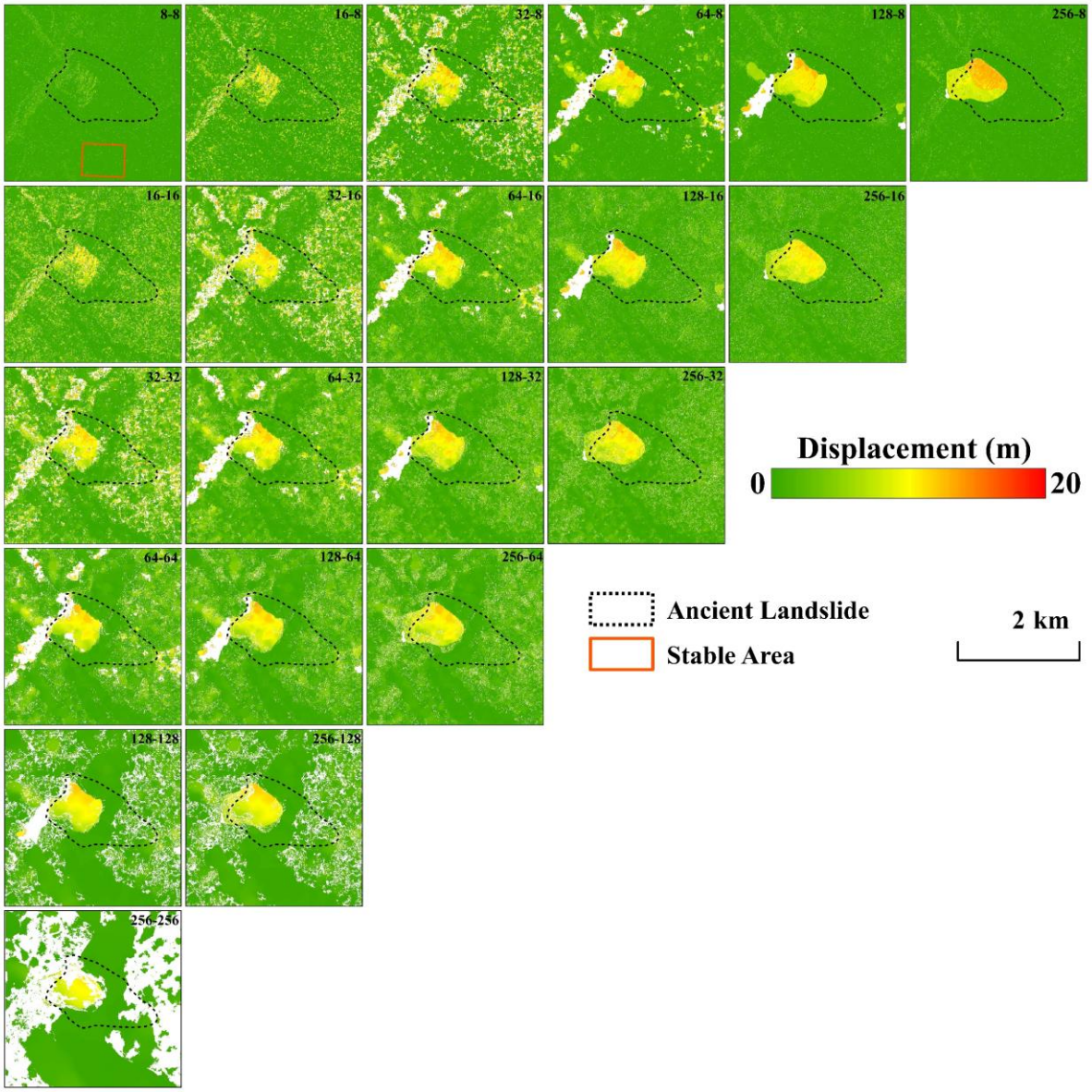


Figure S2. Corrected horizontal displacement mapped from the PlanetScope image pair between 16 June 2020 and 24 June 2020 using different window size combinations (Initial-Final) corresponding to Figure S1.

The mean east-west and north-south displacements derived from the stable area were used to compensate for the misfits, and the overall corrected horizontal displacement can be calculated for different window size combinations. Figure S2 shows the corrected horizontal displacement over the ANZ slope with different combinations of initial and final window sizes. As for the smallest window size combination (initial-final window sizes of 8-8), it failed to detect the spatial pattern and horizontal displacements over the ANZ slope. As the initial-final window sizes were increased, the horizontal

displacements were clearer and more complete spatial distribution of displacements can be detected. For the smaller initial window sizes (16 and 32), more background noise pixels were distributed over the slope. When the initial window size was increased up to 64 or 128, the overall horizontal displacement would be more smooth and lesser background noise pixels were detected. However, as for the largest initial window size (256), the spatial pattern of horizontal displacement was clearly changed to an ellipse-shaped boundary from the top to the bottom, rather than the hourglass-shaped boundary detected from the smaller initial window size (32, 64 and 128). Therefore, it is clearly demonstrated that larger window sizes (64-X, 128-X, and 256-X) would detect displacements clearer by depressing more background noise, but the largest window sizes (256-X) tend to over-smooth the displacements and the spatial patterns were also changed. At the same time, we found that 64-X would capture a more accurate spatial coverage than those from 128-X, as shown in Figure S3. Over the eastern corner of the head scarp labelled with red box, it is clearly shown that the spatial coverage of the 64-X results matched better with the in-field head scarp than the 128-X results. It could be caused by the over-smoothing effect of the large window size. To obtain clear and intact horizontal displacements with relatively low uncertainty, the initial and final window sizes (64-64) were chosen for the subsequent optical POT processing.

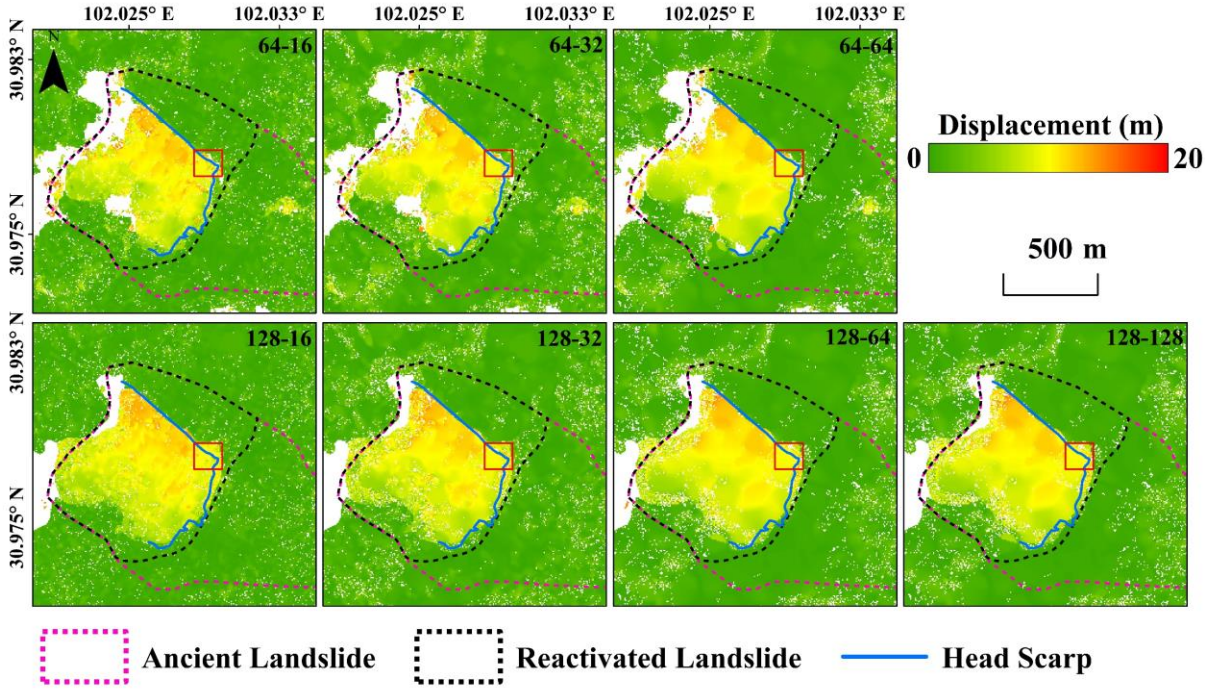


Figure S3. Comparison of horizontal displacements between 64-X and 128-X window size combinations.

Step size test

To further explore the optimal step size for optical POT processing with PlanetScope data, multiple step sizes were tested in this case with the same image pair used in the initial-final window size test. The initial and final window sizes (64-64) was applied in this test owing to the best performance for obtaining the clear and intact horizontal displacements with relatively low uncertainty. Figure S4 shows the mean east-west and north-south displacements and the corresponding standard deviations (uncertainties) in the stable area after the filtering process for different step sizes, as well as the measurement quality (SNR). It is clearly found that the uncertainties of misfits for the larger step sizes (≥ 20) are larger than those for the smaller step sizes (≤ 10). In addition, the misfits and SNR, as well as the corresponding uncertainties, are quite similar for the step sizes of 2, 4, and 6, and the uncertainties for both misfits were all smaller than 0.50 m.

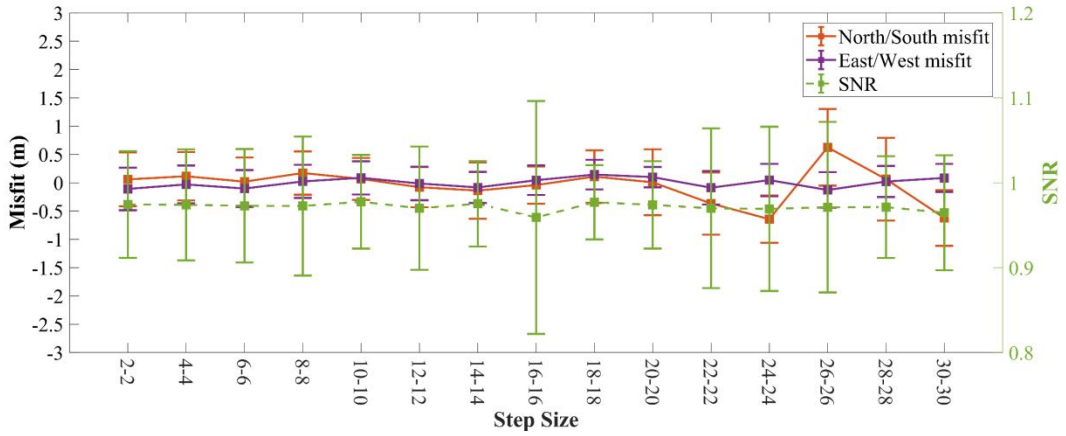


Figure S4. Means, standard deviations, and SNR (measurement quality) in the stable area of POT results derived from the PlanetScope image pair between 16 June 2020 and 24 June 2020 with different step sizes. Note that the fixed initial-final window sizes of 64-64 and red band was used.

The overall corrected horizontal displacements for different step sizes are shown in Figure S5. The boundary of the main landslide body detected from the POT results with smaller step sizes (2, 4, 6, and 8) are much more detailed and smoother than those with larger step sizes. In this case, the POT result with step size of 2 can obtain the most detailed and smooth boundary of main landslide body. At the same time, the tiny deformations can be kept and detected with smaller step size, which could reduce the underestimation of slope displacements. Thus, step size of 2 was chosen based on low uncertainties and more detailed boundary of main landslide body and slope movements for the following optical POT processing.

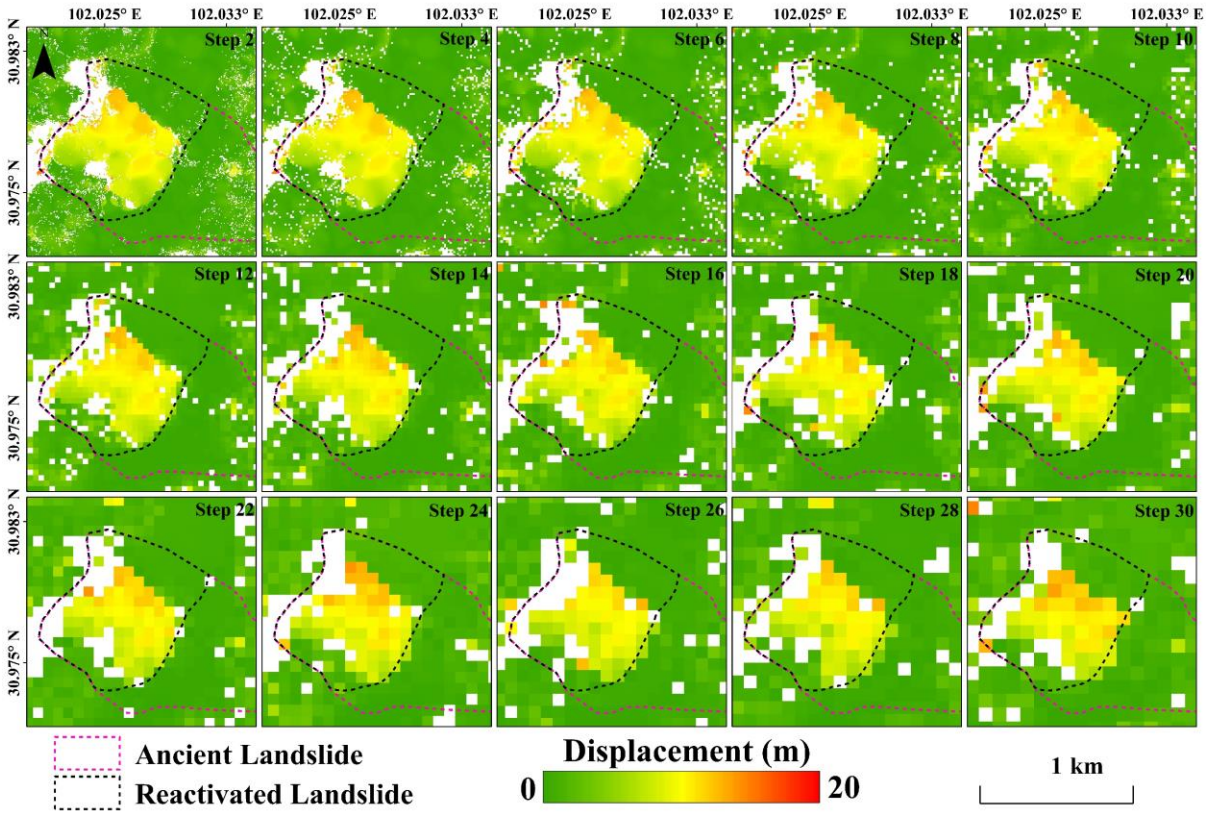


Figure S5. Corrected horizontal displacement mapped from the PlanetScope image pair between 16 June 2020 and 24 June 2020 using different step sizes with the fixed initial-final window sizes of 64-64 and red band.

Band Selection Test

All four bands including blue, green, red, and near infrared (NIR) from the PlanetScope optical images were used for the band selection test to explore the best band for image correlation. We fixed the initial and final window sizes as 64-64 and the step size as 2 in this case. Figure S6 shows the mean East-West and North-South displacements and the corresponding standard deviations (uncertainties) in the stable area after the filtering process for different bands, as well as the measurement quality (SNR). It can be clearly seen that the uncertainties in both misfits for the red band are smaller than those for the other three bands (blue, green, and NIR). That also agreed with the result that red band has the best RMSE in image correlation [34]. Figure S7 also shows the corresponding corrected horizontal displacements for different bands. It is clear that the spatial patterns of horizontal displacements in the middle are

very similar with blue, green, and red bands, while there are two obvious differences detected from the NIR band over the downstream toe and the eastern corner of the middle section. Based on the horizontal displacements retrieved from the very high resolution orthophotos (0.05 m) collected from the unmanned aerial vehicles (UAVs) [34], we found that the spatial pattern of this result agreed well with those retrieved using blue, green, and red in this study. Above all, the horizontal displacements retrieved using the red band in this study presented the best performance with the smallest uncertainties, as well as the more consistent spatial pattern with the result obtained from the unmanned aerial vehicle (UAV) photogrammetry. Thus, we decided to use red band for the optical POT processing in this study.

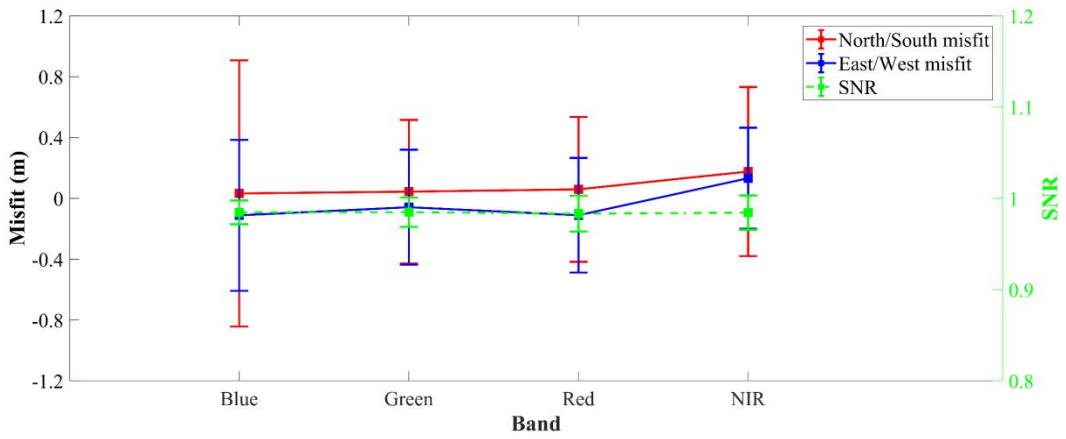


Figure S6. Means, standard deviations, and SNR (measurement quality) in the stable area of POT results derived from the PlanetScope image pair between 16 June 2020 and 24 June 2020 with blue, green, red, and NIR bands. Note the fixed initial-final window sizes of 64-64 and a step size of 2 was used.

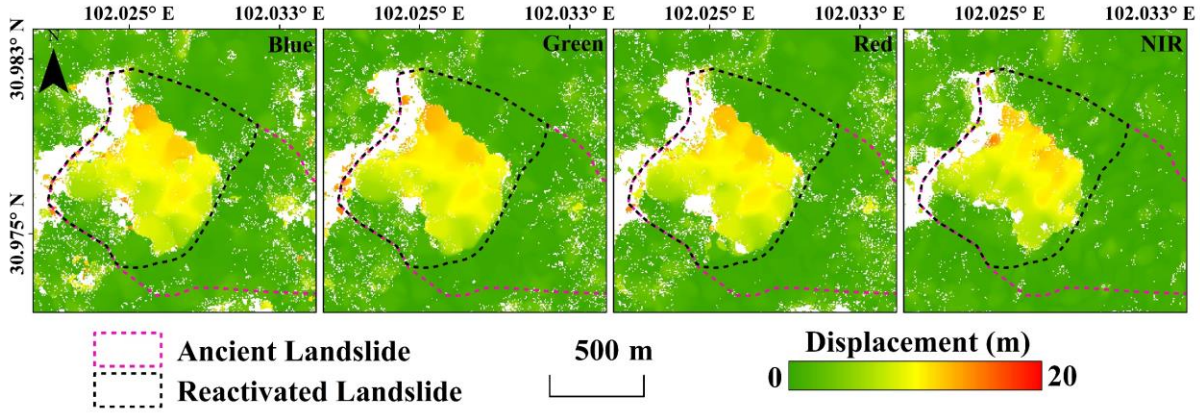


Figure S7. Corrected horizontal displacement mapped from the PlanetScope image pair between 16 June 2020 and 24 June 2020 using different Bands (blue, green, red, and NIR) with the fixed initial-final window sizes of 64-64 and step size of 2.

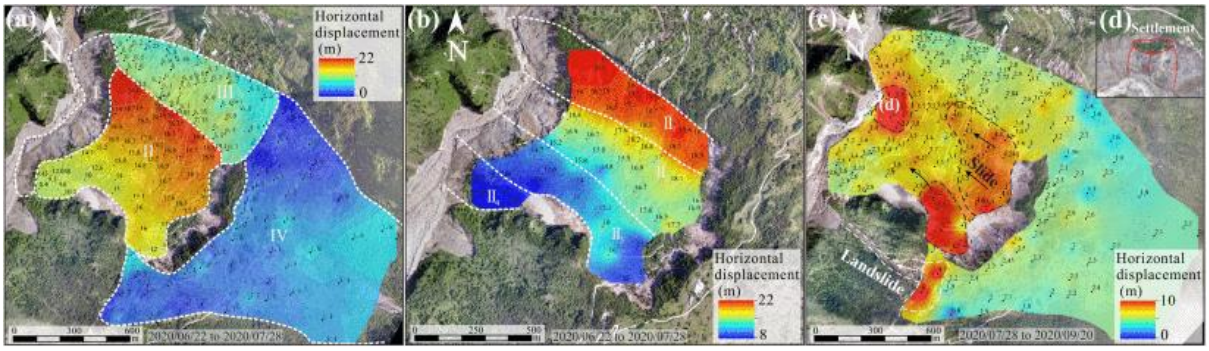


Figure S8. Horizontal displacement of the whole ancient landslide based on difference of orthophotos collected from the unmanned aerial vehicles (UAVs). (a) Horizontal displacement of the whole ancient landslide in the first month. (b) Horizontal displacement of zone II in the first month. (c) Horizontal displacement of the whole ancient landslide in the second and third months. (d) Local subsidence of zone I. Note that this figure is sourced from [13]

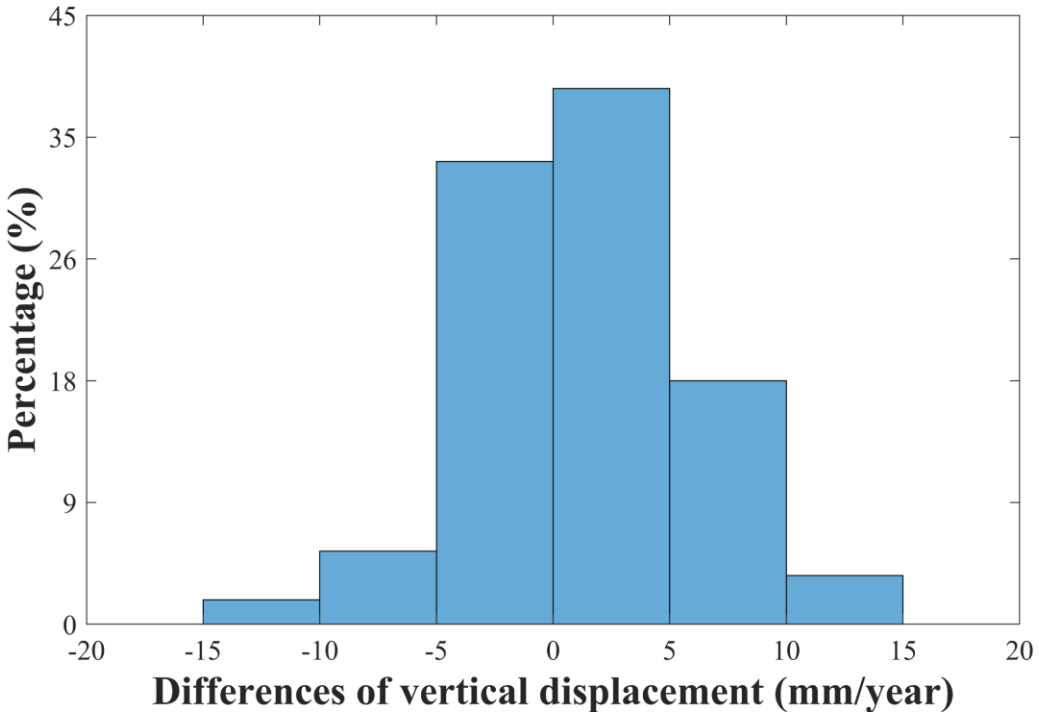


Figure S9. Cross validation based on the differences between the projected vertical displacements from the post-failure descending and ascending InSAR measurements.

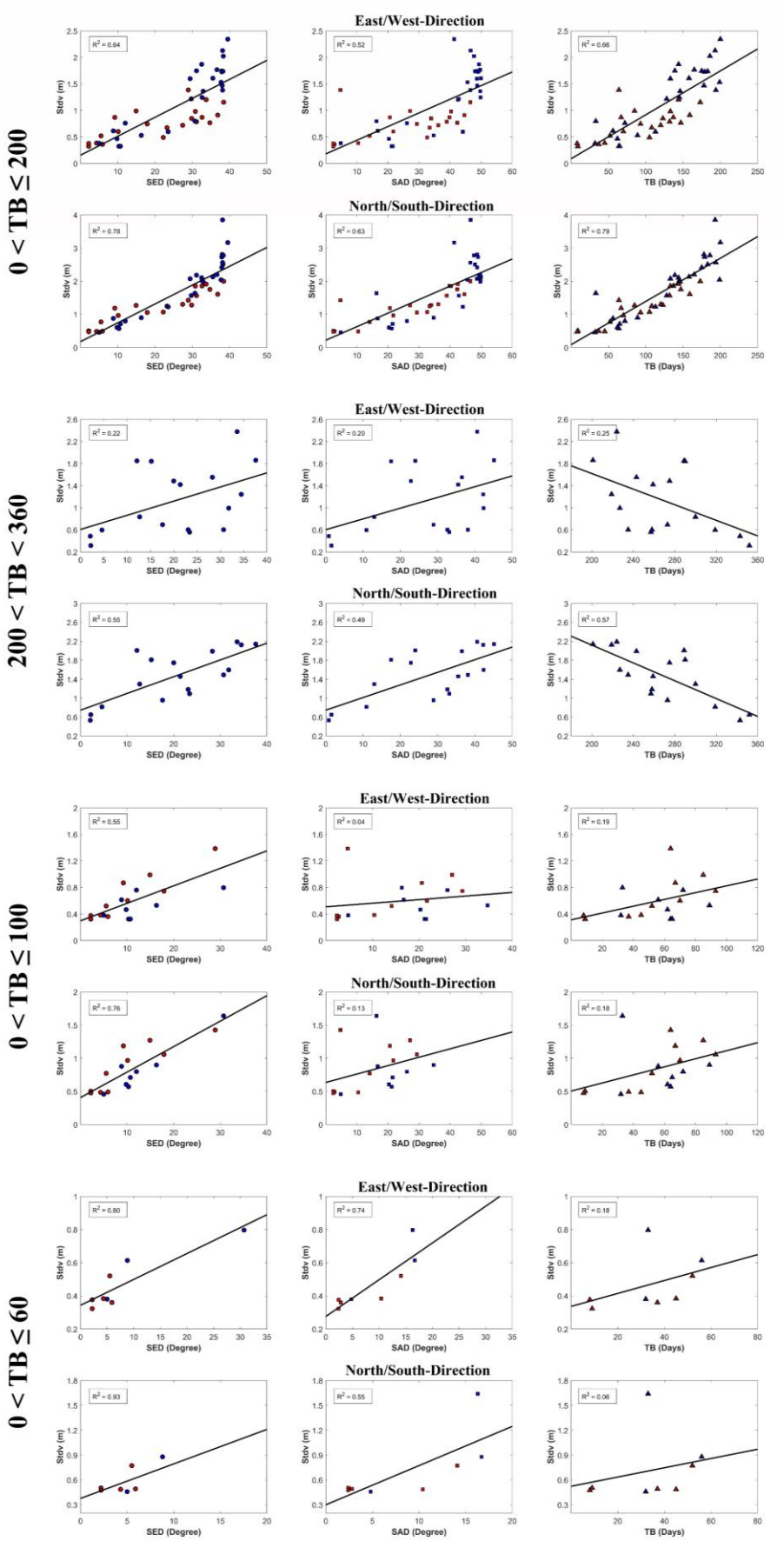

0 < TB ≤ 200
East/West-Direction
North/South-Direction
200 < TB < 360
East/West-Direction
North/South-Direction
0 < TB ≤ 100
East/West-Direction
North/South-Direction
0 < TB ≤ 60
East/West-Direction
North/South-Direction
Stdv (m)
SED (Degree)
SAD (Degree)
TB (Days)
R² = 0.64
R² = 0.52
R² = 0.66
R² = 0.78
R² = 0.63
R² = 0.79
R² = 0.22
R² = 0.20
R² = 0.25
R² = 0.55
R² = 0.49
R² = 0.57
R² = 0.55
R² = 0.04
R² = 0.19
R² = 0.76
R² = 0.13
R² = 0.18
R² = 0.80
R² = 0.74
R² = 0.18
R² = 0.93
R² = 0.55
R² = 0.06

Figure S10. Relationship between SED, SAD, TB, and uncertainties in the East/West direction and North/South direction after imposing limitations to TB ($0 < TB \leq 200$ days, $200 < TB < 360$ days, $0 < TB \leq 100$ days, and $0 < TB \leq 60$ days). The red and blue colour indicate the first and second time series POT results, respectively. The circle, square, and triangle markers represent the SED, SAD, and TB, respectively. The black lines represent the best linear fits.

References

13. Jiang, N.; Li, H.; Hu, Y.; Zhang, J.; Dai, W.; Li, C.; Zhou, J.-W. A Monitoring Method Integrating Terrestrial Laser Scanning and Unmanned Aerial Vehicles for Different Landslide Deformation Patterns. IEEE J. Sel. Top. Appl. Earth Obs. Remote Sens. 2021, 14, 10242–10255.

34. Xia, Z.; Motagh, M.; Li, T.; Roessner, S. The June 2020 Aniangzhai landslide in Sichuan Province, Southwest China: Slope instability analysis from radar and optical satellite remote sensing data. Landslides 2022, 19, 313–329.

50. Yang, W.; Wang, Y.; Wang, Y.; Ma, C.; Ma, Y. Retrospective deformation of the Baige landslide using optical remote sensing images. Landslides 2020, 17, 659–668.